An Exploration of Voltage-Type Rotor Magnetic Field Indirect Vector Control

Yimin Li(✉)

China Airport Construction Group Corporation, Beijing 100010, China
xz2646@sina.com

Abstract. This study primarily delves into the control system of electric braking in urban rail trains, with a particular focus on the asynchronous motor and its associated mathematical model. The investigation embarks upon an exhaustive exploration of two discerning control methodologies: constant voltage-to-frequency ratio control and the rotor magnetic field-oriented vector control method with voltage feedforward decoupling. The culmination of this analysis, coupled with a profound comprehension of the fundamental principles of coordinate transformation, illuminates the intrinsically nonlinear, multivariable essence, and robust coupling characteristics inherent in the asynchronous motor. Through a comparative examination of the two control methods, the constraints of constant voltage-to-frequency ratio control come to the fore, instigating the proposition of a rotor field-oriented vector control strategy. The study reaches its apex with the development of a simulation model, facilitating a comprehensive juxtaposition of the aforementioned control methods. The simulation substantiates the superiority of the vector control method in the context of electric braking control.

Keywords: Electrical automation control · AC speed regulation · Feedforward decoupling algorithm

1 Introduction

Urban rail train's electric braking systems are vital for efficient operation. The AC speed regulation system, lauded for its low cost, simplicity, and stability, is an industry standard, especially for high torque and high capacity situations. It regulates speed through methods like pole-changing, frequency-changing, and slip ratio-changing, with frequency-changing being most effective due to its precise control and energy efficiency.

Speed regulation methods are based on different mathematical models—voltage steady-state model for steady working conditions and voltage dynamic model for dynamic conditions. The squirrel-cage AC induction motor, serving as a vital driving component within the AC speed regulation system, assumes a pivotal role in formulating the mathematical model requisite for governing the braking system [1, 2]. Known for its simple structure, easy maintenance, affordability, and stability, it is commonly employed in AC speed regulation systems.

M. Gong et al. (Eds.): EITRT 2023, LNEE 1138, pp. 106–114, 2024.
https://doi.org/10.1007/978-981-99-9319-2_13

The research paper introduces a method, which harnesses the capabilities of feed-forward decoupling and space vector pulse width modulation technology, thereby showcasing its innovation and effectiveness. This method, by precisely controlling the induction motor, enhances the braking effect significantly. Comparative simulations with the traditional constant voltage-frequency ratio control method demonstrated the new vector control method's superior precision and evident advantages [3].

In summary, AC speed regulation technology, due to its exceptional performance, is pivotal in modern rail transportation. With technological advances, more efficient, stable, and precise speed regulation methods are being developed. The voltage-type rotor magnetic field indirect vector control method, with superior performance, introduces new possibilities for urban rail train's electric braking system. As research deepens and its practical applications increase, this method is expected to revolutionize future electric braking systems.

2 Mathematical Model of an Asynchronous Motor

2.1 The Steady-State Mathematical Model

When the slip rate is very small, we can approximately obtain:

$$T_e = mn_P\left(\frac{U_s}{2\pi f_e}\right)^2 \frac{\omega_s}{R_r} \tag{1}$$

Evident becomes the fact that as the slip frequency s diminishes to a considerable extent, the torque showcases an approximate proportionality to said slip frequency. In the range where $0 <$ slip rate < 1, an asynchronous motor adeptly assumes the guise of a generator, while a negative slip rate signifies the motor's operation. When the slip rate of said asynchronous motor remains minute, the output torque establishes a linear correlation with the slip rate. At a distinct threshold, the torque achieves its utmost pinnacle. However, should the slip rate continue its ascension, the motor's operation descends into an unstable state, resulting in the gradual attenuation of the output torque [4, 5].

2.2 Dynamic Mathematical Model

Asynchronous motors, in juxtaposition to their DC counterparts, exhibit the intrinsic attribute of harboring multiple inputs and outputs. To realize variable voltage and frequency control, the imperative lies in adjusting the relationship betwixt voltage or current and frequency, necessitating the engagement of two autonomous input quantities that remain detached. In tandem with the output variable of speed, equal attention must be devoted to the magnetic flux for comprehensive assessment. The output torque materializes as the outcome of the current and magnetic flux multiplication, while the induced electromotive force emerges from the product of speed and magnetic flux.

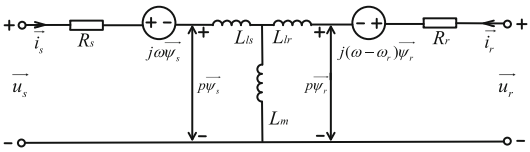

Fig. 1. Equivalent circuit of asynchronous motor based on complex vector

In the course of control transformation, the adoption of the equivalent motor principle ensues, as visually demonstrated in Fig. 1. For the purpose of illustration, let us contemplate the voltage transformation as a striking exemplification:

$$\begin{bmatrix} v_\alpha \\ v_\beta \end{bmatrix} = \begin{bmatrix} \frac{2}{3} & -\frac{1}{3} & -\frac{1}{3} \\ 0 & \frac{1}{\sqrt{3}} & -\frac{1}{\sqrt{3}} \end{bmatrix} \begin{bmatrix} v_a \\ v_b \\ v_c \end{bmatrix} \tag{2}$$

The expression for the inverse transformation is:

$$\begin{bmatrix} v_a \\ v_b \\ v_c \end{bmatrix} = \begin{bmatrix} 1 & 0 \\ -\frac{1}{2} & \frac{\sqrt{3}}{2} \\ -\frac{1}{2} & -\frac{\sqrt{3}}{2} \end{bmatrix} \begin{bmatrix} v_\alpha \\ v_\beta \end{bmatrix} \tag{3}$$

Transformation to two-phase rotating coordinate system:

$$\begin{bmatrix} v_d \\ v_q \end{bmatrix} = \begin{bmatrix} \cos\omega t & \sin\omega t \\ -\sin\omega t & \cos\omega t \end{bmatrix} \begin{bmatrix} v_\alpha \\ v_\beta \end{bmatrix} \tag{4}$$

The expression for the inverse transformation is:

$$\begin{bmatrix} v_\alpha \\ v_\beta \end{bmatrix} = \begin{bmatrix} \cos\omega t & -\sin\omega t \\ \sin\omega t & \cos\omega t \end{bmatrix} \begin{bmatrix} v_d \\ v_q \end{bmatrix} \tag{5}$$

The transformation of the three sets of equations can be achieved as follows:

$$\begin{cases} \vec{u_s} = R_s \vec{i_s} + p\vec{\psi_s} + j\omega\vec{\psi_s} \\ \vec{u_r} = R_r \vec{i_r} + p\vec{\psi_r} + j(\omega - \omega_r)\vec{\psi_r} \end{cases} \tag{6}$$

$$\begin{cases} \vec{\psi_s} = L_s \vec{i_s} + L_m \vec{i_r} \\ \vec{\psi_r} = L_r \vec{i_r} + L_m \vec{i_s} \end{cases} \tag{7}$$

$$\begin{cases} Jp\omega_r/P = T_e - T_L \\ T_e = \dfrac{3P\mathrm{Re}(j\vec{\psi_s}\vec{i_s}^*)}{2} \end{cases} \tag{8}$$

3 Electric Braking Control Methods

3.1 Constant Voltage to Frequency Control Method

As elucidated by the illustrated equivalent circuit in Fig. 1, under the premise of negligible voltage drop across the rotor impedance, the magnetic flux may be deemed invariant, so long as the voltage-to-frequency ratio remains unvarying. This control methodology is denoted as constant voltage-to-frequency control [6].

In this control approach, the maximum torque that an asynchronous motor can generate is synchronized with changes in the stator frequency. However, when the stator frequency is extremely low, both voltage (V) and frequency (f) values become significantly small, contradicting the initial assumptions. To uphold steadfast control of the air-gap flux and sustain the motor's torque output at these meager frequencies, it becomes imperative to implement voltage compensation within the low-frequency spectrum.

When endeavoring to execute speed control of asynchronous motors surpassing the base frequency, the ideal scenario entails an elevation in the output voltage of the inverter to preserve the V/f ratio. However, the constrictions posed by the variable frequency drive's maximal output voltage inhibit the coeval escalation of the stator input voltage in tandem with the ascending stator frequency. As a consequence, the control system is compelled to sustain an unswerving stator voltage while advancing the stator frequency. Such a specific circumstance, wherein the stator voltage perseveres unaltered while the frequency ascends, engenders a decrement in the V/f ratio and subjects the system to a state characterized by a debilitated magnetic field [7].

3.2 Vector Control Method

Within a specific range of speed, stator field-oriented control employs the stator voltage equation to ascertain flux observation, thereby obviating the requirement for rotor parameter estimation. However, its dynamic model succumbs to significant cross-coupling effects, and the decoupling process fails to entirely abolish the influence of rotor parameters, culminating in intricate ramifications. It's also less effective at low speeds due to the impact of stator leakage reactance on the induced electromotive force, making it unsuitable for electric braking systems [8, 9].

Air-gap field-oriented control improves accuracy by inspecting the air-gap flux and effectively controls magnetic flux saturation effects. This makes it suitable for synchronous motors. However, the complexity of control logic increases due to the cross-coupling between flux and slip frequency, limiting its use in electric braking systems.

Rotor field-oriented control effectuates the decoupling of the stator current into discrete excitation and torque components, obviating the requisite for supplementary decouplers. Through the harmonious alignment of the rotor flux with the d-axis within the two-phase rotating coordinate system, a momentous transmutation takes place, facilitating the seamless conversion of three-phase AC quantities into their DC equivalents within the synchronous rotating coordinate system. As a result, the long-awaited AC-to-DC conversion for the AC motor is duly accomplished [10]. This distinctive attribute endows it with an unrivaled aptitude for electric braking control systems.

The fundamental equations governing an asynchronous motor operating under rotor field-oriented control are delineated as follows:

$$\begin{bmatrix} u_{ds} \\ u_{qs} \\ 0 \\ 0 \end{bmatrix} = \begin{bmatrix} R_s + L_s p & -\omega_e L_s & L_m p & -\omega_e L_m \\ \omega_e L_s & R_s + L_s p & \omega_e L_m & L_m p \\ L_m p & 0 & R_r + L_r p & 0 \\ (\omega_e - \omega_r) L_m & 0 & (\omega_e - \omega_r) L_r & R_r \end{bmatrix} \begin{bmatrix} i_{ds} \\ i_{qs} \\ i_{dr} \\ i_{qr} \end{bmatrix} \tag{9}$$

Flux linkage equations:

$$T_r p \psi_r + \psi_r = L_m i_{ds} \tag{10}$$

Electromagnetic torque:

$$T_e = \frac{3PL_m \psi_r i_{qs}}{2L_r} \tag{11}$$

4 Voltage-Oriented Decoupling Algorithm

The goal of this decoupling algorithm is to eliminate the mutual influence between motor currents and enhance the performance and precision of the control system.

4.1 Voltage-Oriented Feedforward Decoupling Algorithm

Voltage-oriented decoupling algorithms commonly encompass a trifecta of techniques: feedback decoupling, cross decoupling, and feedforward decoupling methods [9].

In the realm of feedback decoupling, the voltage decoupling terms come to fruition through the calculated utilization of the stator current components' feedback values, adroitly sieved by a first-order low-pass filter. On the other hand, cross decoupling ingeniously formulates the voltage decoupling terms, drawing inspiration from the outputs of the stator current regulators. Frequency domain analysis of these three voltage-oriented decoupling algorithms reveals that feedforward decoupling has the fastest response, followed by cross decoupling, while feedback decoupling has the slowest response.

For urban rail trains, which are characterized by large inertia and low switching frequency of the power devices, especially under digital control, there can be lag in the response of the axis current controller. Considering the requirements of full electric braking at low speeds, the use of voltage feedforward decoupling control is most suitable for improving the response speed of the vector control system.

By leveraging the system reference values and the actual parameters of the asynchronous motor, the voltage feedforward decoupling terms can be computed in the ensuing manner:

$$\hat{u}_{ds} = R_s i_{ds}^* + \frac{\sigma L_s \Delta i_{ds}^*}{T_s} - \sigma L_s \omega_e i_{qs}^* \tag{12}$$

$$\hat{u}_{qs} = R_s i_{qs}^* + \frac{\sigma L_s \Delta i_{qs}^*}{T_s} + \sigma L_s \omega_e i_{ds}^* + \frac{L_m \omega_e \psi_r^*}{L_r} \tag{13}$$

5 Simulation Verification

The substantial inertia of urban rail train braking systems results in significant instantaneous power during braking. Sustained high current can increase switch losses and place additional demands on the cooling system. Consequently, the system's control frequency must be set at a lower switching frequency. In the simulation model encompassing comprehensive electric braking for urban rail trains, the switching frequency is duly configured at 1 kHz. Algorithms for constant voltage-to-frequency ratio control, vector control, and space vector pulse width modulation are implemented in the C language within the S-function module, outputting six channels of PWM pulse signals. A comparative simulation was performed between the constant voltage-to-frequency ratio control and the indirect vector control method featuring rotor field feedforward decoupling, as shown in Table 1.

Table 1. The simulation experiment parameters

Parameter	Value
Simulation step size	$2e^{-6}$
Interrupt frequency of the DSP	1k
Switching to the braking mode	1.5 s

When switching to the braking mode, it can be observed that the torque response of vector control is significantly higher than that of constant voltage-to-frequency control. In the simulation, the torque in vector control changes almost immediately upon receiving the command, as shown in Fig. 2. The adjustment to the commanded torque typically necessitates approximately 0.5 s in Fig. 3.

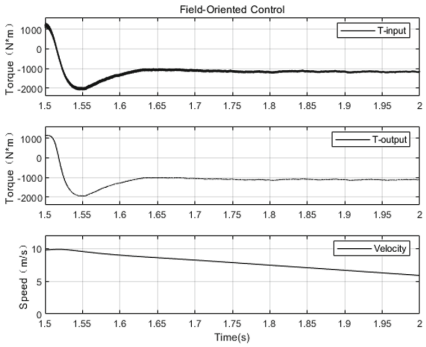

Fig. 2. Vector control waveforms

When switching to the braking mode, both control methods smoothly enter the regenerative braking phase. Within the sphere of vector control, the dynamism exhibited by

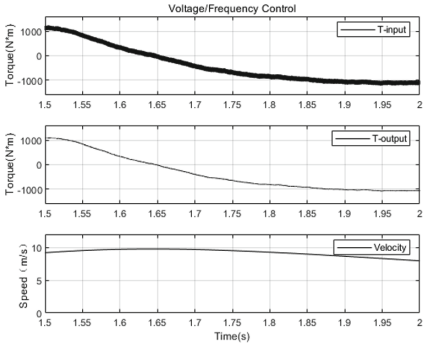

Fig. 3. Voltage-to-frequency control waveforms

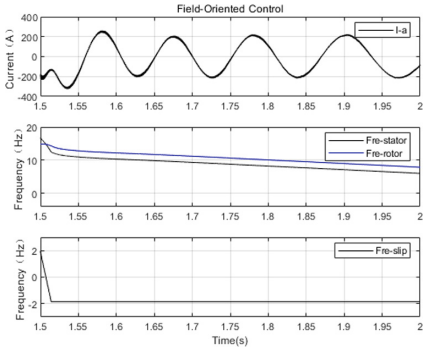

Fig. 4. Vector control waveforms

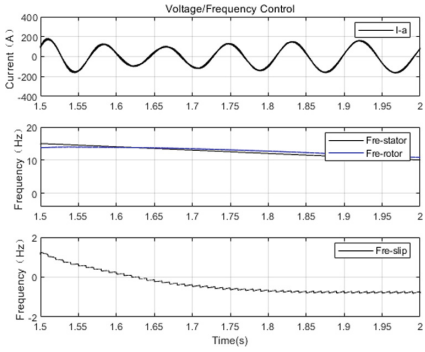

Fig. 5. Voltage-to-frequency control waveforms

the stator frequency surmounts that witnessed in constant voltage-to-frequency control by a notable magnitude, as shown in Fig. 4. Conversely, in the domain of constant

voltage-to-frequency control, the reactivity of the stator frequency materializes as relatively sluggish, while the fluctuation of the slip frequency (s) amplifies noticeably, as exemplified in Fig. 5.

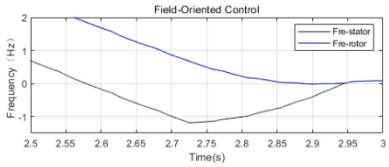

Fig. 6. Vector control waveforms

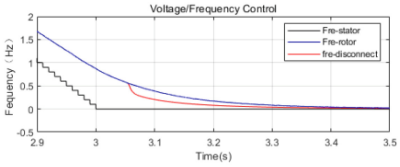

Fig. 7. Voltage-to-frequency control waveforms

As the velocity of the train dwindles and the stator frequency gradually diminishes to zero, the asynchronous motor confronts a predicament in upholding regenerative braking. To perpetually uphold an ample electric braking force, it becomes indispensable to amend the phase sequence of the inverter's three-phase power source, thereby expediting a seamless transition into reverse braking. At this critical juncture, the slip ratio surges beyond 1, enabling the asynchronous motor to harness energy from the inverter, thus preserving a resolute braking force for the braking system. During the braking system switch, to avoid issues such as current shock brought about by the stator frequency passing through the 0 Hz point, the stator frequency is controlled to switch at the natural commutation point, allowing the stator frequency to decrease and automatically cross 0 Hz. Since constant voltage-frequency control cannot naturally commutate, it needs to disconnect the inverter earlier than vector control in low-speed states. It can be seen that disconnecting the inverter allows constant voltage-frequency control to brake and stop the vehicle faster. Vector control can naturally commutate and provide stable braking force during reverse braking at 2.5 s, as shown in Figs. 6 and 7.

6 Conclusion

The study unveils an avant-garde methodology, adeptly incorporating the virtues of feed-forward decoupling and capitalizing on the prowess of space vector pulse width modulation technology to effectively regulate the braking unit of the induction motor. This pioneering approach capitalizes on the inherent advantages of technology, bestowing precise control benefits and thereby augmenting the effectiveness of the braking mechanism. To confirm the superiority of this novel vector control technique, it was

compared with the traditional constant voltage-frequency ratio control method via simulation. The outcomes demonstrate that the new vector control method provides more accurate control and presents clear advantages.

References

1. Deng, L., Mei, H., Zhou, W., et al.: Fitting method of optimal energy-running time curve based on train operation data of an urban rail section. J. Adv. Transp. (2021). https://doi.org/10.1155/2021/6663022
2. Shokhin, V., Kornilov, G.P., Permyakova, O.V., et al.: Investigation of braking modes in the electric drive with direct torque control system. In: International Conference on Industrial Engineering, Applications and Manufacturing (2021). IEEE. https://doi.org/10.1109/ICIEAM51226.2021.9446465
3. Guo, H., Bai, Y., Hu, Q., Zhuang, H., Feng, X.: Optimization on metro timetable considering train capacity and passenger demand from intercity railways. Smart Resilient Transp. **3**(1), 66–77 (2021). https://doi.org/10.1108/SRT-06-2020-0004
4. Luo, Y., Ma, H., Xu, G., et al.: A new type of motor load model for vehicle TCS/ABS test. In: IEEE International Conference on Information and Automation (2017). IEEE. https://doi.org/10.1109/ICInfA.2017.8078900
5. Malhotra, A., Gaur, P.: Comparative study of dc-dc converters in solar energy systems. In: International Conference on Advances in Computing (2014). IEEE. https://doi.org/10.1109/ICACCI.2014.6968374
6. Sebaa, K., Zhou, Y., Li, Y., et al.: Low-frequency oscillation damping control for large-scale power system with simplified virtual synchronous machine. J. Modern Power Syst. Clean Energy **99** (2021). https://doi.org/10.35833/MPCE.2020.000340
7. Zhang, L., Bai, J., Wu, J.: Speed sensor-less control system of surface-mounted permanent magnet synchronous motor based on adaptive feedback gain supertwisting sliding mode observer. Hindawi Limited (2021). https://doi.org/10.1155/2021/8301359
8. Tan, Q., Wei, R., Wang, X., et al.: Traction-system research based on different proportion of current in double-end supply for high-speed maglev. In: 2017 20th International Conference on Electrical Machines and Systems (ICEMS) (2017). IEEE. https://doi.org/10.1109/ICEMS.2017.8056261
9. Hou, G., Zhao, Z., Bai, X., et al.: Fuzzy immune PID control used in no-load grid-connection for doubly-fed wind power system. In: Proceeding of the 11th World Congress on Intelligent Control and Automation. 0[2023-06-16]. https://doi.org/10.1109/WCICA.2014.7053230
10. Zhan, C., Zhu, L., Zhang, Y., et al.: A novel sensor-less on-line estimation method of IGBT junction temperature. In: IEEE Energy Conversion Congress & Exposition—Asia (2021). IEEE. https://doi.org/10.1109/ECCE-Asia49820.2021.9479058